Polyether phases of Formic acid revealed under high pressure

Himal Bhatt*[1, 2], Ashok K. Verma*[1, 2] and P. Modak[1, 2]

[1]High Pressure & Synchrotron Radiation Physics Division, Bhabha Atomic Research Centre, Mumbai-400 085, INDIA

[2]Homi Bhabha National Institute, Anushaktinagar, Mumbai-400 094, INDIA

Electronic Supplementary Information (ESI)

1. First principles evolutionary crystal structure searches and molecular dynamics simulations:

Extensive first-principles evolutionary crystal structure searches were carried out at 10, 20 and 50 GPa using simulation cells of 1-4 formula units of formic acid with the help of USPEX code[1-3]. Over the years, this method has been established as a versatile tool for predictions of novel stoichiometries and crystal structures of materials at high pressures.[4-8] In recent times, this method was also used successfully to predict the crystal structures of molecular system.[9-17] As usual, first generation of structures was generated randomly and then these structures were fully optimized. Initial population sizes were taken 10-40 depending on total number of atoms in the unit cells. In these searches, the plane-wave basis set was generated by taking a 500 eV energy cutoff and the reciprocal space integrations were performed by employing Monkhorst-Pack method[18] with a grid spacing of $2\pi \times 0.04$ Å^{-1}. Energetically favorable structures were re-optimized by using a better set of computational parameters. In this set of calculations the plane-wave basis set energy cutoff was set 600 eV and reciprocal space

integration was done with a grid spacing of $2\pi \times 0.02$ Å^{-1}. Effect of the computational parameters was carefully analyzed and the chosen parameters insured the convergence of total energies better than 1.0 meV per atom. Positions of ions were relaxed until the forces on them became smaller than 2.0 meVÅ^{-1}. For all calculations, we used Perdew-Burke-Ernzerhof version of the exchange-correlation.[19] For structure searches, we used the VASP code[20–22] and projector augmented wave (PAW) potentials. Evolution of the structures was monitored at various pressures, with final enthalpy values re-computed using quantum-espresso code[23]. For this, we used ultrasoft pseudopotentials which were taken from the PSlibrary[24], with an energy cutoff of 80 Ry and reciprocal space integrations were performed using a k-point grid of spacing $2\pi \times 0.02$ Å^{-1}. The van der Waal corrections were included in the calculations using the DFT-D2 method of Grimme et al.[25] For MD simulations, Γ-point was used for Brillouin zone sampling and time-step was taken 1 femto-second. All simulations were performed for 10 ps using ambient structure unit cell. Also, MD simulations taking larger supercell (2×2×2) were carried out at ambient pressure to test the validity of our results on bond distributions (both OH covalent and H---O HB). The initial 3 ps data was discarded and a total of 7000 equilibrated configurations were used for analysis of bond-lengths. All the structure models were rendered using VESTA software.[26]

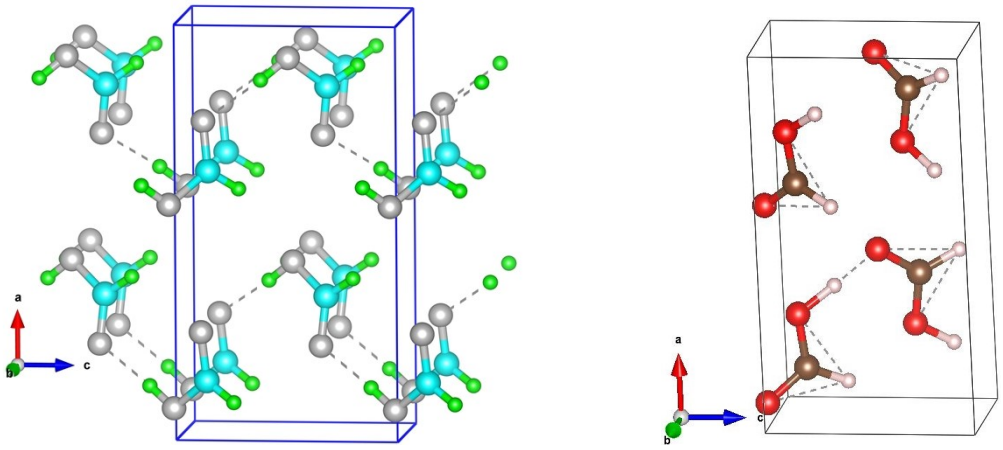

Figure S1. Crystal structure of Formic acid (projection in *ac*-plane): Orthorhombic **(left)** *cis* $Pna2_1$ (also shown in main text) and **(right)** *trans* $Pna2_1$ in the low pressure phase.

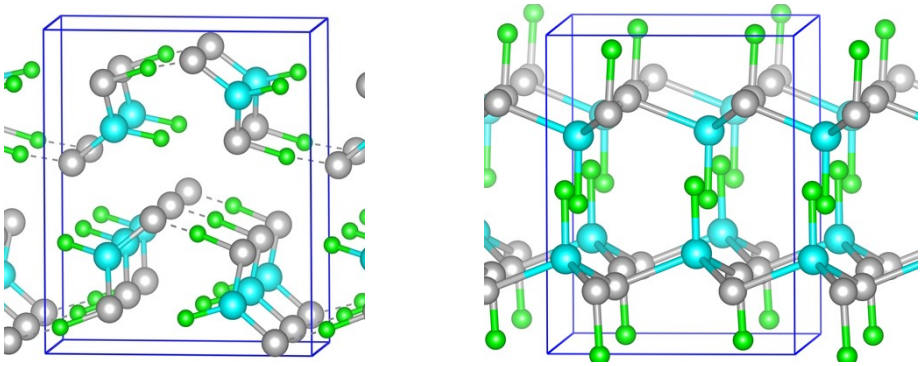

Figure S2. Possbile crystal structures of Formic acid (projection in *ac*-plane) near 20 GPa: **(left)** orthorhombic *trans* $P2_12_12_1$ and **(right)** *polymer* - $Pca2_1$ (also shown in main text).

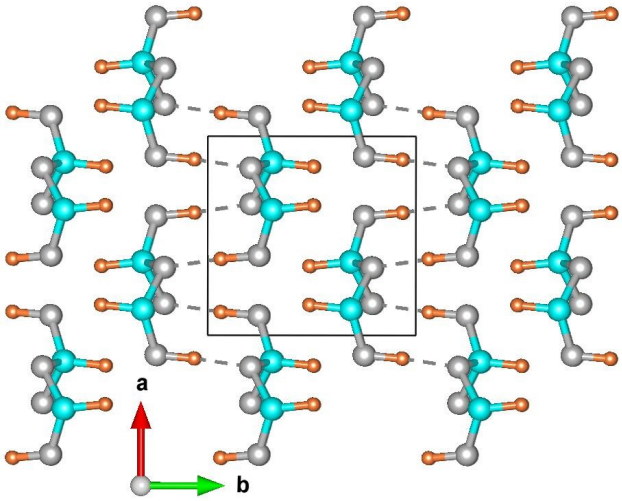

Figure S3. Another orientation of *polymer* - *Pca*2_1 crystal structure of Formic acid above 20 GPa. The polymer chains along *c*-axis are inter-connected by strong hydrogen bonds nearly along the *b*-axis forming bilayers in the *ab*-plane. The bilayers are further connected by weaker hydrogen bonds.

Table S1. Some molecular parameters of formic acid at various pressures

Pressure (GPa)	**Conformation**	**O-H (Å)**	**H---O (Å)**	**O---O (Å)**	**∠OHO (degree)**
0 (SG33- *Pna*2_1)	*cis*	1.05	1.49	2.54	175.72
10 (SG33- *Pna*2_1)	*cis* *trans*	1.11 1.09	1.30 1.33	2.41 2.43	176.41 175.49
20 (SG33- *Pna*2_1)	*cis* *trans*	1.134 1.130	1.246 1.25	2.378 2.379	175.94 175.93
20 (SG19- *P*$2_1$$2_1$$2_1$)	*trans*	1.13	1.24	2.36	168.55
20 (SG29- *Pca*2_1)	*poly*	1.00	1.51	2.51	176.7
30 (SG29- *Pca*2_1)	*Poly (intrabilayer)*	1.00	1.46	2.46	177.24
60 (SG79- *I*4)	*Poly - rings*	1.03	1.40	2.33	147.20

Table S2. Fully optimized crystal structures of the Formic acid (Here van der Waals interactions were included):

Space group	Pressure	Lattice parameters (Å)	Wyckoff positions
$P2_12_12_1$ No.: 19	25 GPa	a = 6.8624 b = 2.8247 c = 5.8411	C :4a: 0.1870, 0.7394, 0.7533 O1 :4a: 0.0757, 0.8290, -0.0819 O2 :4a: 0.3382, 0.4843, 0.7761 H1 :4a: 0.1097, 0.6340, 0.0992 H2 :4a: 0.1514, 0.8784, 0.8867
$Pca2_1$ No.: 29	20 GPa	a = 5.0090 b = 5.3466 c = 4.0616	C :4a: 0.6266, 0.3133, 0.1202 O1 :4a: 0.6537, 0.2119, 0.8042 O2 :4a: 0.3940, 0.2441, 0.2472 H1 :4a: 0.6202, -0.0578, 0.7731 H2 :4a: 0.6470, 0.5155, 0.1139
$I4$ No.: 79	60 GPa	$a = b$ = 6.9401 c = 3.8823	C :8c: 0.4986, 0.2556, 0.3907 O1 :8c: 0.0083, 0.7575, 0.2392 O2 :8c: 0.3369, 0.3370, 0.2574 H1 :8c: 0.8849, 0.8351, 0.3187 H2 :8c: 0.5007, 0.1110, 0.2941

2. *High Pressure Infrared Spectroscopic Studies*:

High pressure infrared spectra of crystalline formic acid, formed upon compression of liquid in a diamond anvil cell (DAC) (as in ref.[27-30]) were measured at various pressures. The signal to noise ratio of the spectra, recorded in reflectance mode, was poor at lower pressures and improved significantly at higher pressures. However, the transmission spectra were saturated, as also reported in some previous reports. The recorded reflectance data after normalization for

background and DAC contribution are shown in Figure S4. Some of the selected reflectance data are also shown in the main text. The spectra were recorded using Bruker Vertex 80V FTIR spectrometer equipped with KBr beamsplitter and liquid nitrogen cooled HgCdTe detector. Both, synchrotron source (100 mA, 0.45 GeV) as well as thermal source were used. A Bohler Almax plate DAC with type IIa IR diamonds of culet size 500 μm was used for measurements in a Hyperion 2000 microscope coupled with the spectrometer. The sample was loaded in a 240 μm thick SS gasket pre-indented to a thickness of 60 μm. Pressure calibration was done using Ruby fluorescence. The data were modeled using a coupled oscillator model shown by solid lines in Figure S4 to determined real optical conductivity at various pressures. Approximate oscillator positions in the diamond absorption and far IR regions were assumed using ref.[28, 30]. The soft mode behaviour reported in ref.[28] could be followed up to nearly 16 GPa. The irregularities in the observed spectra up to this pressure could be explained using the conventional mode - coupling scheme.

At lower pressures, various subtle changes in our IR spectra as well as the previously reported indicate the conformational transition above 4.5 GPa in FA. Strengthening of the hydrogen bond results in the softening of νC=O mode (stretching; ~ 1630 cm^{-1}). Figure 4b (main text) shows that this mode shows a minimum at 4.5 GPa, followed by broadening,[28] similar to the νC=O Raman mode behavior seen in ref.[29]. This implies the emergence of *trans* conformer with differing bond parameters. A peak broadening in the δCO2 (deformation) mode near 700 cm^{-1} above 4.5 GPa in both IR and Raman spectra[28] is also consistent with the above inference. A rise in IR intensity at 1200 - 1300 cm^{-1} region in the reported low pressure spectra above 4 GPa,[28] can easily be correlated with the emergence of the characteristic fingerprint mode δCOH-CO of *trans* FA.[31-32]

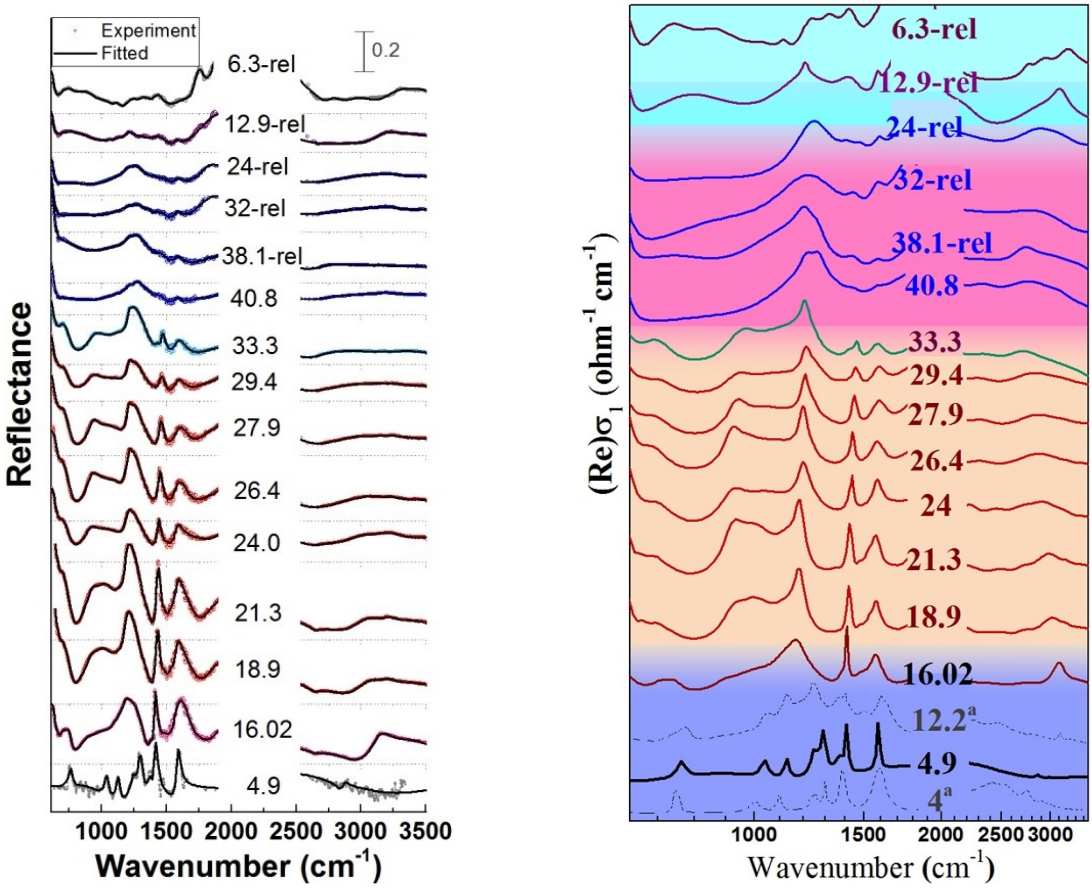

Figure S4: High pressure IR spectra of crystalline formic acid **(left)** Normalized reflectance data (circles) for diamond and other contributions. The data were modeled using a coupled oscillator model shown by solid lines. **(right)** The determined real optical conductivity at various pressures. Dotted patterns[a] are traces obtained from ref.[28], showing a good match. Some of these data have also been shown in main text.

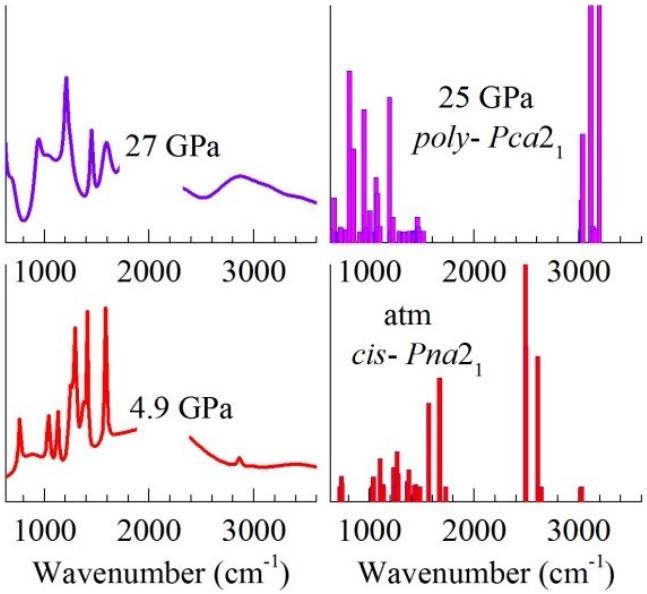

Figure S5: Comparison of the **(left)** experimentally obtained high pressure IR spectra of formic acid at 4.9 GPa and 27 GPa with **(right)** IR modes calculated using density functional perturbation theory, as implemented in the QE code, at ambient pressure in a $Pna2_1$ structure and at 25 GPa in a $Pca2_1$ structure. Among other important signatures, the evolution of polyether modes in 900 - 1200 cm^{-1} spectral region and new O-H stretching signatures in 3000 cm^{-1} spectral region are significant findings verifying the phase transition above 20 GPa.

Table S3: The most intense IR and Raman active modes of a simple polyether POM (polyoxymethylene)[33-36] composed of repetitive ⊦C-O-C⊣-units.

	Crystalline POM[33]		Trigonal POM single crystal[34] (0.45 GPa)				Orthorhombic POM crystal[34] (>2 GPa)				Extruded POM[35]	POM fiber Melt spin[36]	High Pressure polymer of FA [our work]	
			Needlelike - extended chain		Lamellar-folded chain		Needlelike extended chain		Lamellar folded chain		IR reflection	IR absorption	20 GPa	dv/dp (19-34 GPa) (cm^{-1}/GPa)
	IR	Raman	IR	Raman	IR	Raman	IR	Raman	IR	Raman			IR	
v_{sym} COC	903 vvs 932 vvs	919 s	897 935	919	1002 935	919	936 895	918	936 987	918 909	904 949	901	925	1.73
v_{asym} COC	1091 vvs 1097 vvs		1097		1092 1136		1096 1133		1121 1108		1108 1140	1135	1170	2.67

Table S4: Comparison of observed (27GPa) and calculated (25GPa) prominent IR modes of FA

	Calculated mode position (relative intensity) (cm^{-1})	Experimentally observed (cm^{-1})
δCO_2 (in plane) δCO_2 (out of plane)	641 661 720	692
δ (COH + CH)	808 844	820
ν_sCO (chain mode)	946	936
δC-OH	1003 1061	1026
δCO2 + CH	1075	
ν_aCO + δOCH (chain mode)	1097 1189 1223	1188 1206
δCH	1456 1467	1449
δ (COH + CO)	1512	1580
νOH	3021 3034	2918
νOH + νCH	3110	3090
νCH	3134	
νCH + νOH	3154 3193	3166 3387

Table S5: Formic acid computed phonon frequencies at Γ- point for SG33 and SG29 at 25 GPa

SG33:

Mode No.	ω (cm^{-1})	IR Intensity	Raman Intensity
1	0	0	0
2	0	0	0
3	0	0	0
4	87.21	0	1.0896
5	118.09	0.1917	0.0184
6	125.73	0.0529	0.8684
7	141.21	0	5.6438
8	184.96	0.0706	0.9796
9	189.34	1.2294	12.792
10	202.54	0	4.8621
11	204.35	0.0014	0.8616
12	260.64	21.1365	7.3369
13	263.89	0	0.5396
14	285.2	0.971	0.452
15	290.05	1.7602	0.2698
16	293.19	0	0.1702
17	356.66	0	1.8092
18	390.42	0.1522	9.9503
19	397.14	20.4618	36.0725
20	406.95	39.5269	15.6034
21	413.56	7.8742	0.628
22	440.62	24.0435	10.5509
23	460.58	0	3.2967
24	494.42	0.0868	3.0608
25	731.16	20.369	53.0385
26	737.17	6.0927	0.4529
27	787.37	0	0.7567
28	792.72	16.0929	2.7758
29	1050.48	39.3872	3.2664
30	1050.76	171.8817	68.8323
31	1067.5	1.8012	0.3946
32	1070.46	0	10.738
33	1081.77	2.472	42.2058
34	1083.39	2.2726	9.7739
35	1228.56	1.139	34.5807
36	1230.74	26.8356	0.1402
37	1255.67	0.4751	1.5885
38	1256.78	0	0.7397
39	1324.36	0	0.4002

40	1341.85	1.5393	23.0796
41	1366.68	0.3295	111.3999
42	1382.15	46.3201	76.8985
43	1387.51	0.2375	6.5767
44	1391.44	0	4.4112
45	1411.1	3.3918	0.6181
46	1413.54	14.53	455.9692
47	1432.63	59.124	45.1123
48	1530.09	0	4.506
49	1540.41	44.0005	7.5772
50	1573.49	8.114	1.2347
51	1653.1	13.9118	0.7662
52	1665.85	0	11.7727
53	1826.13	43.2156	51.9866
54	1872.92	4.8472	6.1463
55	1899.72	91.612	20.7229
56	1990.77	0	19.5206
57	3217.79	2.2918	1038.0582
58	3219.17	0	75.1304
59	3219.44	0.759	337.1563
60	3219.99	1.0136	142.7398

SG29:

Mode No.	**ω (cm^{-1})**	**IR Intensity**	**Raman Intensity**
1	0	0	0
2	0	0	0
3	0	0	0
4	117	0.0889	1.3609
5	141.11	0.0623	1.1992
6	141.51	0	0.8975
7	235.16	0.8467	0.0999
8	257.9	0	2.8529
9	302.58	1.3568	2.1807
10	310.51	0.034	0.0071
11	363.19	0	0.0621
12	368.66	0.0471	1.3855
13	408.59	1.6292	0.0388
14	408.68	0	0.0029
15	417.94	0.2276	0.5064
16	444.91	0.0395	6.2949
17	543.25	0.4665	52.0153
18	595.5	0.0087	0.0424
19	641.64	0.6873	1.4646

20	661.53	8.9932	5.2538
21	690.09	0	1.0999
22	699.63	0.0362	0.8131
23	718.14	0	0.0828
24	720.97	1.2334	2.9132
25	775.28	0.6538	0.1109
26	808.48	42.6819	1.6792
27	844.18	21.9502	12.0333
28	908.26	0	1.8842
29	946.56	32.3049	5.6496
30	967.54	1.1147	0.0952
31	1003.55	5.5235	0.6855
32	1014.75	0	4.3657
33	1057.64	0	2.4427
34	1061.08	14.4626	0.9151
35	1075.8	10.2532	69.8542
36	1097.25	1.4142	0.7628
37	1189.67	35.6127	2.1331
38	1197.29	0	0.0014
39	1223.41	3.8243	7.8661
40	1280.3	0.1901	0.0424
41	1325.87	5E-4	67.5713
42	1330.48	0.0028	5.3238
43	1373.68	0.0142	0
44	1377.51	0	46.8584
45	1379.07	0.1002	38.3173
46	1417.13	0.2647	0.1941
47	1429.29	0.0365	3.0433
48	1447.59	0	16.9334
49	1456.3	3.7916	7E-4
50	1467.93	1.2724	9.0079
51	1480.86	0	35.5001
52	1512.33	0.1113	4.223
53	3021.48	8.2821	1644.691
54	3026.36	0	182.7568
55	3034.57	25.8967	39.6965
56	3110.52	150.8017	9.3148
57	3134.15	1.2863	7.3541
58	3136.03	0	12.2571
59	3154.95	0.7109	633.5191
60	3193.44	75.9392	45.187

Figure S6: Some prominent IR modes of FA in the polymeric phase above 20 GPa. Here, cyan ball represents C-atom, grey ball O-atom and small green ball H-atom.

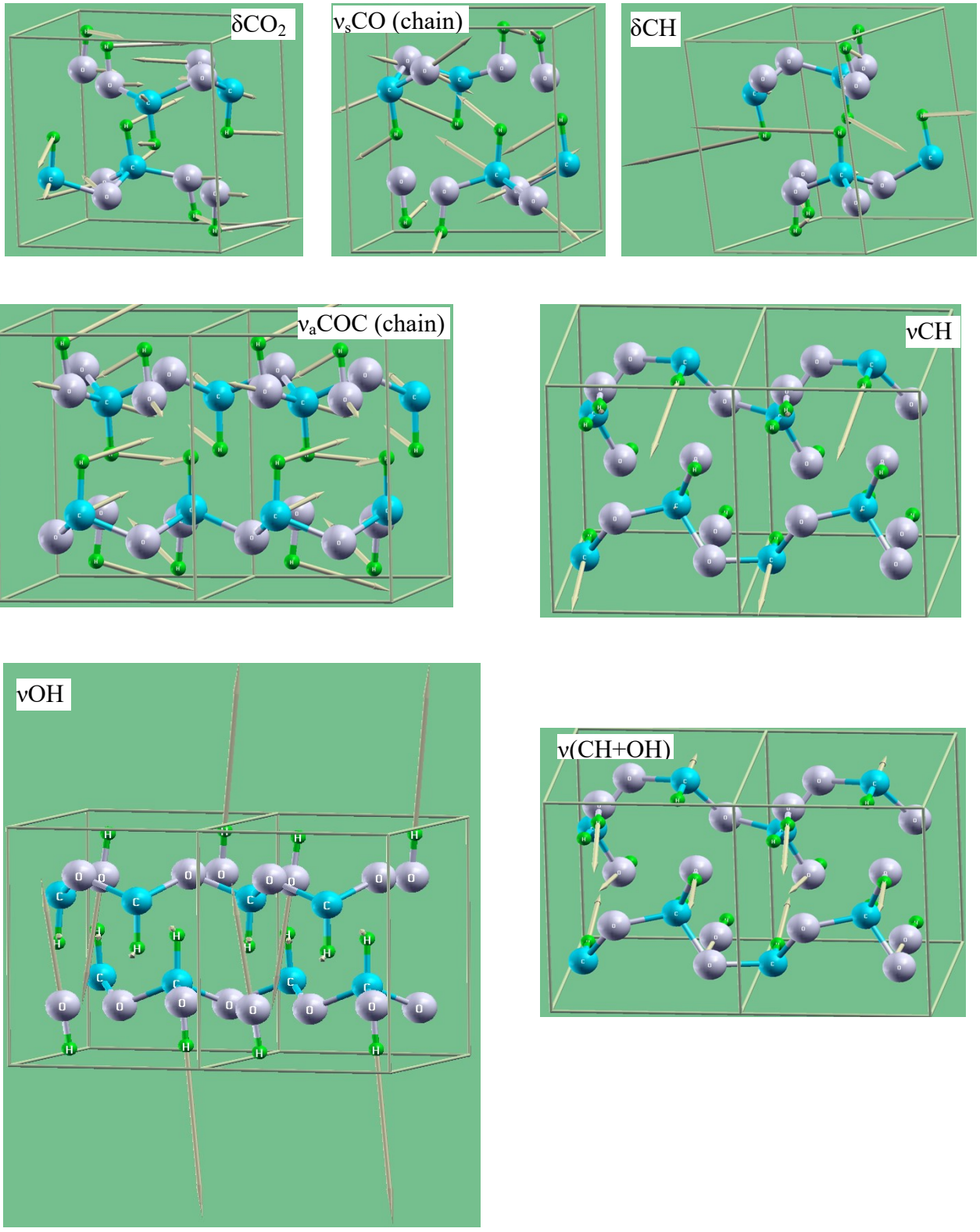

References:

(1) A. R. Oganov and C. W. Glass, J. Chem. Phys. **124**, 244704 (2006).

(2) A. O. Lyakhov, A. R. Oganov, H. T. Stokes, and Q. Zhu,Comput. Phys. Commun. **184**, 1172 (2013).

(3) A. R. Oganov, A. O. Lyakhov, and M. Valle, Acc. Chem. Res. **44**, 227 (2011).

(4) A. R. Oganov and S. Ono, Nature (London) **430**, 445 (2004).

(5) P. Modak and A. K. Verma, Phys. Chem. Chem. Phys. **21**, 13337 (2019).

(6) A. K. Verma and P. Modak, Phys. Chem. Chem. Phys. **20**, 26344 (2018).

(7) A. K. Verma, P. Modak, and L. Stixrude, Amer. Mineral. **103**, 1906 (2018).

(8) A. K. Verma, P. Modak, and S. M. Sharma, J. Alloys Compd.**710**, 460 (2017).

(9) A. S. Naumova, S. V. Lepeshkin, P. V. Bushlanov and A. R. Oganov, J. Phys. Chem. A **125**, 3936−3942 (2021).

(10) Guang-Rui Qian, A. O. Lyakhov, Q. Zhu, A. R. Oganov and X. Dong, Sc. Rep. **4**, 5606 (2014).

(11) E. Stavrou, A. A. Maryewski, S. S. Lobanov, A. R. Oganov, Z. Konôpková, V. B. Prakapenka and A. F. Goncharov, J. Chem. Phys. **155**, 184503 (2021).

(12) J. K. Hinton, S. M. Clarke, B. A. Steele, I-Feng W. Kuo, E. Greenberg, V. B. Prakapenka, M. Kunz, M. P. Kroonblawd, E. Stavrou, CrystEngComm **21**, 4457-464 (2019).

(13) G. Gao, A. R. Oganov, Y. Ma, H. Wang, P. Li, Y. Li, T. Iitaka and G. Zou, J. Chem. Phys. **133**, 144508 (2010).

(14) A. R. Oganov, Faraday Discuss., **211**, 643 (2018).

(15) G. Saleh1 and A. R. Oganov, Sc. Rep.**6**, 32486 (2016).

(16) Xiao-Dong Wen, R. Hoffmann and N. W. Ashcroft, J. Am. Chem. Soc. **133**, 9023–9035 (2011).

(17) Q. Zhu and S. Hattori, J. Mat. Res., **38**, 19-36 (2023).

(18) J. P. Perdew, K. Burke, and M. Ernzerhof, Phys. Rev. Lett. **77**, 3865 (1996).

(19) G. Kresse and J. Hafner, J. Phys.: Condens. Matter **6**, 8245 (1994).

(20) P. E. Blöchl, Phys. Rev. B **50**, 17953 (1994).

(21) G. Kresse and J. Furthmüller, Comput. Mater. Sci. **6**, 15 (1996).

(22) G. Kresse and D. Joubert, Phys. Rev. B **59**, 1758 (1999)

(23) P. Giannozzi et al 2009 J. Phys. Condens. Mat. **21**1

(24) A. Dal Corso, Computational Material Science 95, 337 (2014).

(25) S. Grimme, J. Antony, S. Ehrlich and H. Krieg, J. Chem. Phys 132, 154104 (2010)

(26) K. Momma and F. Izumi, J. Appl. Crystallogr. **44**, 1272 (2011).

(27) D. R. Allan and S. J. Clark, Physical Review Letters 82, 3464 (1999).

(28) A. F. Goncharov, M. R. Manaa, J. M. Zaug, R. H. Gee, L. E. Fried, and W. B. Montgomery, Physical Review Letters 94, 065505 (2005).

(29) H. Shimizu, Physica B+C 139-140, 479 (1986).

(30) V. W. Manner, R. S. Chellappa, S. A. Sheffield, Z. Liu, and D. M. Dattelbaum, Applied Spectroscopy 67, 1080 (2013).

(31) M. Pettersson, J. Lundell, L. Khriachtchev, and M. Räsänen, Journal of the American Chemical Society 119, 11715 (1997).

(32) J. D. Goddard, Y. Yamaguchi, and H. F. Schaefer III, The Journal of chemical physics 96, 1158 (1992).

(33) Y. Matsui, T. Kubota, H. Tadokoro, and T. Yoshihara, Journal of Polymer Science Part A: General Papers 3, 2275 (1965)

(34) M. Kobayashi, H. Morishita, and M. Shimomura, Macromolecules 22, 3726 (1989)

(35) N. Nagai, H. Okada, Y. Amaki, M. Okamura, T. Fujii, T. Suzuki, A. Takayanagi, and S. Nakagawa, AIP Advances 10, 095201 (2020)

(36) L. Li et al., Polymers for Advanced Technologies 26, 77 (2015)